Nanoscale

PAPER

View Article Online
View Journal | View Issue

Cite this: *Nanoscale*, 2014, **6**, 11932

A stretchable strain sensor based on a metal nanoparticle thin film for human motion detection†

Jaehwan Lee,‡[a] Sanghyeok Kim,‡[a] Jinjae Lee,[a] Daejong Yang,[ab] Byong Chon Park,[c] Seunghwa Ryu[a] and Inkyu Park*[ab]

Received 15th June 2014
Accepted 11th August 2014

DOI: 10.1039/c4nr03295k

www.rsc.org/nanoscale

Wearable strain sensors for human motion detection are being highlighted in various fields such as medical, entertainment and sports industry. In this paper, we propose a new type of stretchable strain sensor that can detect both tensile and compressive strains and can be fabricated by a very simple process. A silver nanoparticle (Ag NP) thin film patterned on the polydimethylsiloxane (PDMS) stamp by a single-step direct transfer process is used as the strain sensing material. The working principle is the change in the electrical resistance caused by the opening/closure of micro-cracks under mechanical deformation. The fabricated stretchable strain sensor shows highly sensitive and durable sensing performances in various tensile/compressive strains, long-term cyclic loading and relaxation tests. We demonstrate the applications of our stretchable strain sensors such as flexible pressure sensors and wearable human motion detection devices with high sensitivity, response speed and mechanical robustness.

1. Introduction

Recently, there has been growing interest in human-friendly electronic devices such as flexible batteries,[1,2] stretchable circuits[3–5] and flexible sensors.[6–9] Specifically, wearable strain sensors attached on the clothing or human body could be used as a human motion detector in medical (*e.g.* rehabilitation assistance and personal health monitoring),[10,11] sports (*e.g.* performance monitoring and novice training)[12,13] and entertainment fields (*e.g.* immersive games and motion capture for movie and animation). In human motion detection, the strain sensor has to satisfy the following requirements: high stretchability, flexibility, sensitivity, durability and fast response/recovery speeds. Among these requirements, high stretchability is very important for detecting a large range of human motions. However, conventional strain gauges using rigid materials such as metal thin foil or silicon piezoresistors have limited stretchability (ε_{max} < 5%). Therefore, various kinds of strain sensing materials such as carbon nanotube/polymer (PDMS),[14–18] carbon black/thermoplastic elastomer,[19] graphene/epoxy,[20] silicon nanomembrane/polymer (Ecoflex)[21] and ZnO nanowire/polystyrene nanofiber hybrid structures[22] have been studied for advanced strain sensors with high stretchability. However, aforementioned studies require multi-step fabrication processes including the time-consuming synthesis process of sensing materials or the metallization process under tightly restricted vacuum conditions. Also, most studies have focused on the sensing of tensile strain, not the compressive strain.

In this work, we present a new type of stretchable strain sensor with high sensitivities not only to tensile but also to compressive strains. Using single-step direct transfer patterning, ion-based metal nano-ink was transferred from the donor substrate to the micro-structured PDMS stamp and used as a sensing material as well as an electrode, which is a very simple and low-cost process. The fabricated strain sensor based on the micro-cracks of a metal nanoparticle thin film on the PDMS stamp can be stretched up to 20% strain with high durability and high strain sensitivity. Also, we demonstrated that the fabricated strain sensor could be used as a wearable human motion detection device for fingers and wrists. In addition, a flexible pressure sensor with high sensitivity as well as fast response and recovery to the low pressure (<1 kPa) was implemented by using stretchable strain sensing elements.

2. Experimental

2.1 Strain sensor based on an Ag NP thin film

As the first step, the mixture of a PDMS pre-polymer and a curing agent (Sylgard 184, Dow corning, USA) with a weight ratio of 10 : 1 was poured on the silicon mold with the SU-8 10 negative photoresist patterned by a conventional photolithography process. After curing in a convection oven at 65 °C for 4 h, micro-structured PDMS stamps with a thickness of 1 mm and a

[a]*Department of Mechanical Engineering, Korea Advanced Institute of Science and Technology (KAIST), Daejeon, 305-701, Korea. E-mail: inkyu@kaist.ac.kr; Tel: +82-42-350-5240*

[b]*KI for the NanoCentury & Mobile Sensor and IT Convergence (MOSAIC) Center, KAIST, Daejeon, 305-701, Korea*

[c]*Korea Research Institute of Standard and Science, Daejeon, 305-340, Korea*

† Electronic supplementary information (ESI) available. See DOI: 10.1039/c4nr03295k

‡ These authors equally contributed to this work.

step height of 10 μm were detached from the silicon mold. Then, an ion-based Ag nano-ink (TEC-IJ-040, Inktec, Korea) was spin-coated at 5000 rpm for 30 s on a piece of silicon (3×3 cm^2) as a donor substrate. The concentration and viscosity of Ag nano-ink are 20 wt% and 15 cP, respectively. Then, the PDMS stamp was pressed by a nominal pressure of ~30 kPa onto the donor substrate with spin-coated Ag nano-ink film for 20 s. Here, the PDMS stamp was used as both the stamp for transferring of Ag nano-ink and the target substrate. After detaching the PDMS stamp from the donor substrate, it was annealed in the convention oven at 140 °C for 20 min for removing the organic solvent and making conductive connections between Ag NPs by sintering. During this process, ionic Ag nano-ink was transformed into a solidified Ag NP thin film (see Fig. 2a). The sizes of annealed Ag NPs range from 25 to 35 nm, with an average diameter of 28.5 nm and a standard deviation of 3.1 nm. The mechanism of Ag nano-ink transfer from the donor substrate to micro-structured PDMS is the cohesive failure of Ag NP nano-ink solution.[23] The adhesive energy between the Ag nano-ink and the donor substrate and that between the Ag nano-ink and PDMS are both larger than the cohesive energy of the Ag nano-ink. Therefore, partial transfer of the Ag nano-ink to PDMS occurs by inner breaking behavior of Ag nano-ink (see ESI, Fig. S1†). The fabricated strain sensor was etched by using a focused ion beam (FIB) in order to observe the cross-section of the Ag NP thin film on the PDMS substrate. The electromechanical characteristics of the packaged strain sensor were measured by using a motion controller (PMC-1HS, Autonics Corp., Korea) and a potentiostat (CHI601D, CH Instruments, Inc., USA).

2.2 Motion detection glove

The fabricated strain sensors were attached on the forefinger and middle finger parts of a rubber glove. Then, strain sensors were connected with a Lab-View based multi-channel data acquisition system (National Instruments, USA). The electrical resistance of the integrated sensors was continuously measured and monitored in real-time.

2.3 Flexible pressure sensor

Thin PDMS membranes were fabricated by conventional spin coating on a silicon substrate with PR patterns followed by a thermal curing process. An Ag NP pattern was printed on the PDMS membrane by using the single-step direct transfer process mentioned above. The PDMS membrane with a serpentine Ag NP pattern was aligned and bonded onto a PDMS block with a center hole as shown in Fig. 6a.

3. Results and discussion

Many previous studies have reported that microscale cracks are created in the metal thin films on the elastomeric substrate during the deposition/transfer processes.[18,23–25] Although these metal thin films with initial micro-cracks on the elastomeric substrate have high electrical resistance, they are stretchable maintaining the electrical conductance under tensile strain cycles. In the work by S. P. Lacour *et al.*[18] and I. M. Graz *et al.*[24] the mechanisms of stretchability of cracked metal thin films on an elastomeric polymer were explained. When the metal thin film on an elastomeric polymer is stretched, the local strain on the metal thin film is not high enough to make plastic deformation of metal ligament networks due to the twisting and out-of-plane deflection of the metal networks. Therefore, the resistance of the metal thin film is increased by the opening of micro-cracks during the elongation cycle but then recovered by their closure during the release cycle. The working principle of our stretchable strain sensor based on the Ag NP thin film with micro-cracks is also the stretchability of the Ag NP thin film as shown in Fig. 1a. When a tensile strain is applied to the sensor, initial micro-cracks are enlarged in a perpendicular direction to the stretch. Here, the electrical current path becomes narrower and longer due to the hindrance by the increased micro-cracks. As a result, the resistance of a strain sensor is increased under the stretching process. After the release of strain (*i.e.* $\varepsilon = 0\%$), micro-cracks are close to the initial state and the resistance of a strain sensor is recovered (see ESI, Fig. S2†). *In situ*, low-vacuum (~0.2 mbar) mode scanning electron microscopy (SEM) images of the Ag NP thin film on the PDMS substrate under tensile strains are shown in Fig. 1b. At $\varepsilon = 20\%$, a number of initial micro-cracks and newly created micro-cracks by the applied strain were opened with widths from tens of nanometers to a few hundreds of nanometers in a perpendicular orientation to the direction of elongation. After releasing the Ag NP thin film from strain (*i.e.* $\varepsilon = 0\%$), the orientations of micro-cracks became random and their widths became greatly reduced. Also,

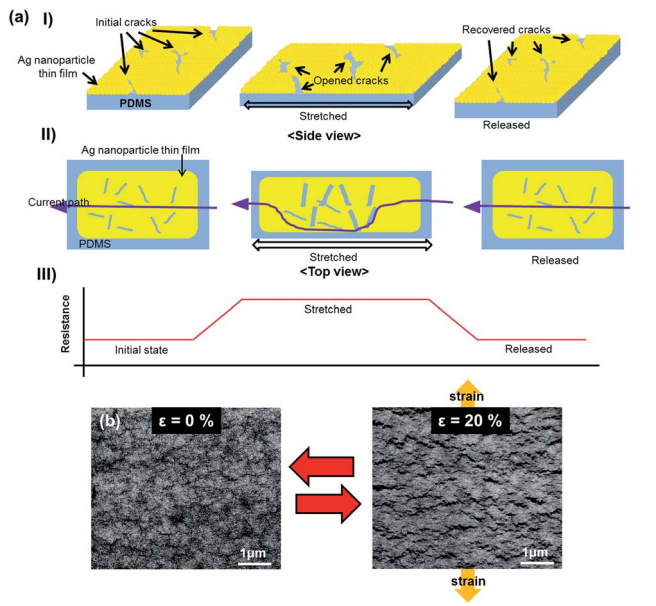

Fig. 1 (a) Working principle of a stretchable strain sensor: (i) an Ag NP thin film on the PDMS substrate during an elongation/relaxation cycle, (ii)–(iii) change in the current path and resistance of the Ag NP thin film during an elongation/relaxation cycle; (b) environmental SEM images of micro-cracks on the Ag NP thin film at $\varepsilon = 0\%$ and $\varepsilon = 20\%$, respectively; A number of micro-cracks opened at $\varepsilon = 20\%$ by a tensile load as compared to the relaxation status ($\varepsilon = 0\%$) of the sensor.

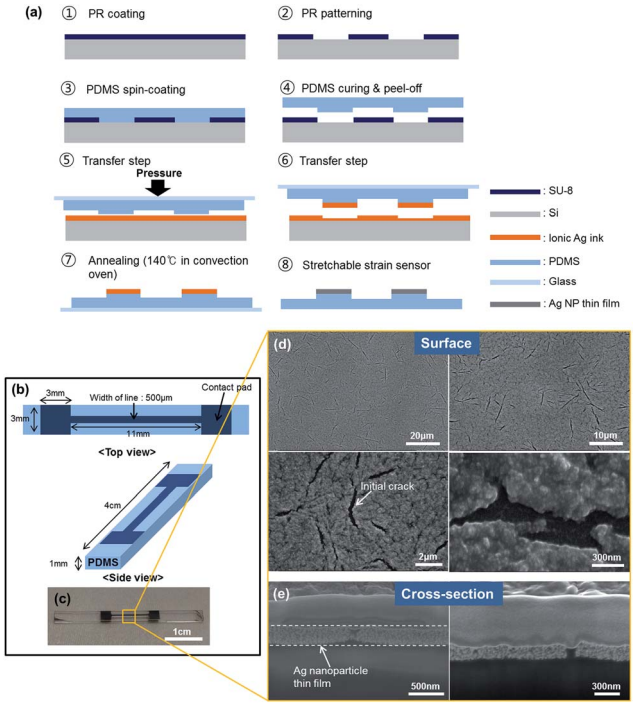

Fig. 2 (a) Fabrication process of the Ag NP-based stretchable strain sensor by using single-step direct transfer printing on the PDMS substrate, (b)–(c) schematic and photograph images of the fabricated strain sensor, (d)–(e) SEM images of the surface and cross-section of transferred Ag NP thin films on the PDMS substrate; initial micro-cracks were created on the Ag NP thin film during the annealing process due to the difference of thermal expansion coefficient between the Ag NP thin film and PDMS as well as the shrinkage of the film during the formation of Ag NPs from ionic solution.

the surface of the micro-cracks on the Ag NP thin film during an elongation/relaxation cycle was observed by using Atomic Force Microscopy (AFM) (see ESI, Fig. S3†).

As mentioned above, the sensor was fabricated by a very simple process based on the single-step direct transfer patterning of ion-based metal nano-ink from the donor substrate to the micro-structured PDMS stamp (see Fig. 2a). The schematic diagrams and the photograph of the fabricated strain sensor are shown in Fig. 2b and 2c. The SEM images of the surface and cross-section of the Ag NP thin films on the PDMS substrate in Fig. 2d and 2e reveal that many initial micro-cracks exist on the surface of the Ag NP thin films. The average thickness of the Ag NP thin film from 7 measurement spots was 356 nm with a standard deviation of 75 nm. Due to the significant difference of the thermal expansion coefficient (α) between the Ag NP thin film (bulk silver: $\alpha = 18.9\ \mu m\ m^{-1}\ K^{-1}$) and PDMS (Sylgard 184: $\alpha = 310\ \mu m\ m^{-1}\ K^{-1}$), numerous initial micro-cracks were created during the annealing process. In order to evaluate the electrical characteristics of the fabricated Ag NP thin film on the PDMS substrate, we measured the current–voltage (I–V) characteristics and resistivity using the 4 point probe measurement method. Ag NP thin films showed a typical ohmic resistor behavior with an average resistivity (ρ) of $6.67 \times 10^{-6}\ \Omega$ m, which is ~400 times higher than that of bulk Ag ($\rho = 1.6 \times 10^{-8}\ \Omega$ m). This high resistivity was caused by a porous structure and numerous initial micro-cracks on the surface of the Ag NP thin film. Since the as-deposited thin film is made by coating of ionic ink, it is totally nonconductive and thus its conductivity cannot be measured before the annealing process.

Environmental factors such as humidity, temperature, and physical damage can affect the characteristics of the strain sensor. Therefore, the fabricated strain sensor on the PDMS stamp was covered by a 0.4 mm thick PDMS encapsulation layer except the contact pad areas to prevent the influence of environment factors (Fig. 3a and b). As shown in Fig. 3c, strains from 0% to 20% with an incremental step of 5% (dwelling period = 10 s and a strain rate of 1% per s for each step) were applied to the strain sensor. The sensor showed linearity to the applied strains with a little hysteresis during the recovery process. However, the sensor showed slower recovery time periods than a fast response to elongation. During the loading/unloading cycles of elastomer materials, residual strain can be generated after the unloading process of the stretched elastomer due to the residual stress.[26,27] Therefore, these experimental results may be caused by the hysteresis and residual strain of the PDMS substrate. The change of the normalized resistance ($\Delta R/R_0$) was from 0.06 ($\varepsilon = 5\%$) to 0.41 ($\varepsilon = 20\%$) with a maximum gauge factor (GF) of 2.05 at $\varepsilon = 20\%$. The change of electrical resistance can be attributed to the widening of the initial micro-cracks as well as the creation of new micro-cracks during the elongation process. On the other hand, opened initial and newly created micro-cracks become smaller and close to the initial state during the strain release process due to the elasticity of PDMS substrate, resulting in the recovery of resistance.

A strain sensor has to maintain its sensing characteristics without fatigue failure for real-life applications. To investigate the long-term stability of the strain sensor, 1000 cycles of repeated stretching/releasing with a maximum strain of $\varepsilon = 10\%$ was applied to the sensor at a strain rate of $\pm 2.5\%$ per s for 8000 s (Fig. 3d). The strain sensor showed good stability with the maximum change of the normalized resistance ($\Delta R/R_0$) of 0.24 during 1000 cycles of stretching/releasing without failure. From this experimental result, we could verify that our strain sensor has good mechanical durability against repeated elongation/relaxation cycles such as human motion, despite a certain level of long-term drifting. Also, 10% strain was applied to the strain sensor at a strain ramping rate of 1% per s and maintained for 10 min and 1 h, respectively, in order to observe the drifting characteristics of the sensor under static loading (Fig. 3e and f). Under a constant strain of $\varepsilon = 10\%$, the drifts of electrical resistance of the strain sensor were only 1% for 10 min and 1.5% for 1 h.

In addition to the sensing characteristics under tensile loading, the sensing performance of the sensor was investigated under compressive loading. As shown in Fig. 3g, two sets of compressive loading cycles composed of four different compressive strains ($\varepsilon = -0.8\%$, -1.6%, -2.9% and -3.6%; strain rate = 1% per s), 10 times each, were applied to the strain sensor by bending motion. In the first cycle, the change of the

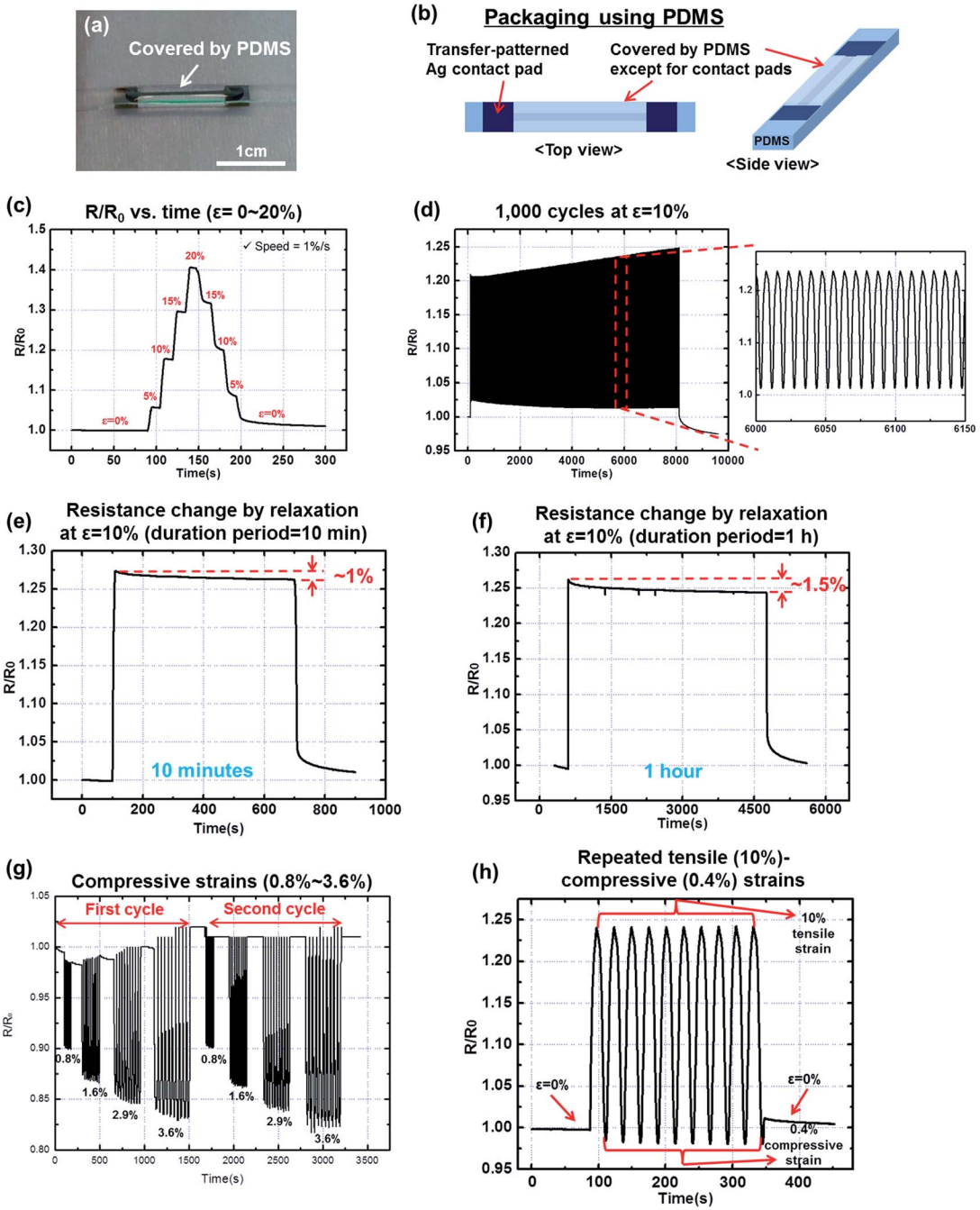

Fig. 3 (a)–(b) Photograph and schematic images of the strain sensor packaged by a PDMS cover; sensing performances of the sensor under (c) a cycle of strain from $\varepsilon = 0\%$ to $\varepsilon = 20\%$ and (d) 1000 cycles of elongation/relaxation at $\varepsilon = 10\%$; drift characteristics of the sensor under a constant strain at $\varepsilon = 10\%$ for (e) 10 min and (f) 1 h; sensing performances of the sensor under (g) various compressive strains (0.8%, 1.6%, 2.9%, and 3.6%) and (h) repeated cycles of tensile (10%)/compressive (0.4%) strains.

normalized resistance ($\Delta R/R_0$) was increased from -0.10 at $\varepsilon = -0.8\%$ to -0.17 at $\varepsilon = -3.6\%$ with increasing compressive strains. It is believed that the initial micro-cracks on the Ag NP thin film causing the high resistance of the film[28] became smaller or closed by the compressive loading, improving the electrical contacts between neighboring Ag NPs. The maximum and minimum GF's for compressive strains were 12.5 at $\varepsilon = -0.8\%$ and 4.7 for $\varepsilon = -3.6\%$. In the second set of compressive loading, the sensor showed a similar sensing performance as the first set. Furthermore, we could verify that the sensor exhibited repeatable and stable responses to the repeated stretching ($\varepsilon = 10\%$) and compression ($\varepsilon = -0.4\%$) cycles as shown in Fig. 3h. Many strain sensors previously developed have shown no or little sensitivity to the compressive strains[16] and therefore required two different sensors for detecting positive and negative strains. On the other hand, our sensor can be used for detecting both positive and negative strains from various human motions.

In order to understand the opening/closure behavior of micro-cracks on the Ag NP thin film by stretching/releasing processes, we conducted a numerical simulation. In our model, the adhesion between NPs is described as elastic bonds with maximum allowable strains, and the adhesion between NPs and the substrate is described in a similar manner. The following assumptions and conditions were used for the numerical simulation in order to capture the experimental conditions: (a) the bonding stiffness between Ag NPs is assumed to be uniform; (b) maximum allowable strains between NPs before bond breaking are randomly distributed. If the strain between NPs exceeds the maximum value, a cohesion force between NPs disappears; (c) each Ag NP is attached to the substrate until the force between the NP and the substrate is smaller than a critical value, and separated if the force exceeds the critical value; (d) the substrate is described as a perfect isotropic elastic medium within the strain range considered in this study. The Ag NP thin film was stretched up to $\varepsilon = 25\%$ and then released to $\varepsilon = 0\%$ as shown in Fig. 4a. During the elongation process, the initial micro-cracks were opened and propagated through the Ag NP network, resulting in larger and longer micro-cracks and higher electrical resistance at higher strains. Then, stretched Ag NP thin films were released to the initial state when the strain returns to $\varepsilon = 0\%$. During the strain release process, the strains between Ag NPs were decreased and became smaller than the maximum allowable strain. This allows most Ag NPs to rebond with their neighboring NPs. Therefore, most opened micro-cracks were closed again and the electrical resistance was recovered close to the initial value at $\varepsilon = 0\%$. Here, it should be noted that a very small increase of resistance from the initial value occurs (4.90% for the Ag NP thin film with initial cracks and 3.18% for the Ag NP thin film without initial cracks) since a very small fraction of NPs is not completely closed again. Fig. 4b shows the numerical simulation result of the Ag NP thin film with and without initial cracks. During the entire stretching/releasing process, the rate of change in resistance of the Ag NP thin film with initial cracks was larger than that of the Ag NP thin film without initial cracks. The stress concentration near initial crack tips fosters the debonding between NPs, which results in the larger resistance change compared to the film without initial cracks. Therefore, the Ag NP thin film strain sensor with initial cracks could be more sensitive to the applied strain. These numerical simulation results show good agreement with the opening/closure behavior of the micro-cracks on

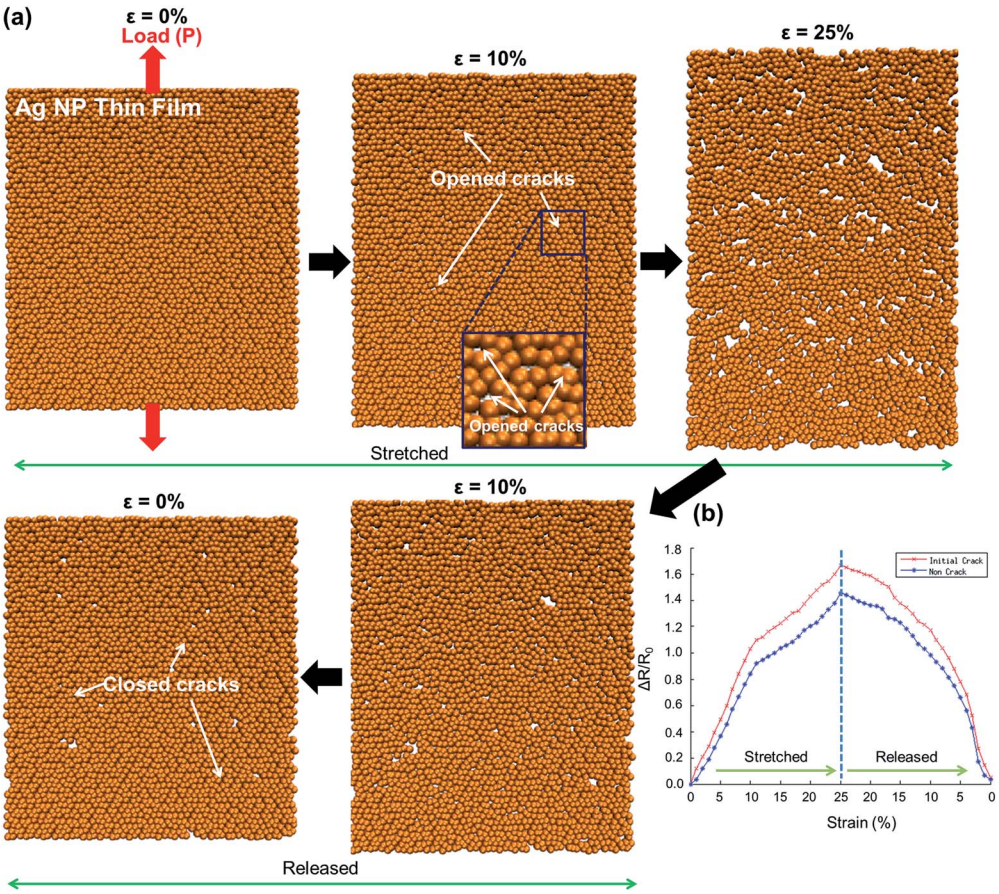

Fig. 4 (a) Results of molecular dynamics based numerical simulation for the Ag NP thin film under elongation/relaxation processes; during the elongation process by the external load, micro-cracks were opened and propagated at higher strains. During the relaxation process, opened micro-cracks become smaller and closed with decreasing strains; (b) relative change of electrical resistance of the Ag NP thin film with and without initial micro-cracks under the stretching/releasing process calculated by numerical simulation.

the Ag NP thin film as the working principle of the developed strain sensor.

The size of the cracks or pores can affect the electrical characteristics of the Ag NP thin films. The pore-induced strain concentration can accelerate the initiation of microcracks.[29] Also, we have shown that Ag NP thin films with larger surface pores showed larger and longer cracks by tensile loading, resulting in poor electromechanical characteristics.[28] In addition, we conducted more in-depth numerical simulations of electrical resistivity of the Ag NP thin film (see Fig. S4†). We described the Ag NP thin film with a bead-and-spring model, in which a broken bond is equivalent to a microcrack with the size of a NP diameter. To study the effect of the number and size of microcracks to the electromechanical responses, we considered the following four cases: without cracks (A), 5% of randomly broken bonds (B), 20% of randomly broken bonds (C), and 15% of broken bonds where we always break a cluster of 3 neighboring bonds together (D). Thus, (C) has 4 times more microcracks with the same size compared to (B). In contrast, (D) has the same number of microcracks but the size of each microcrack is 3 times bigger than that of (B). As shown in Fig. S4,† during the entire stretching/releasing process, the rates of change in the resistance of (C) was larger than those of (A) and (B). Also, (D) showed higher $\Delta R/R_0$ than those of (A) and (B). The maximum $\Delta R/R_0$ at $\varepsilon = 25\%$ were 1.45 (A), 1.67 (B), 2.50 (C), and 2.64 (D), respectively. Therefore, we could conclude that the Ag NP thin film shows higher sensitivity to the applied tensile strain when the size of individual cracks is larger or the total number of cracks is higher.

Since the developed strain sensor has great advantages such as mechanical flexibility, bendability and high strain sensitivity, they can be used for the human motion detection.[10–13] In this work, we used our Ag NP-based strain sensor for detecting the motions of human fingers and the wrist. As shown in Fig. 5a, we developed a motion detection glove integrated with strain sensors on the finger joints. Fig. 5b shows the sensing performance of the motion detection glove for different finger motions. During the bending/relaxation motion of the forefinger, the resistance of the forefinger sensor (#1) was increased and recovered. During this period, the middle finger sensor (#2) did not show any response. On the other hand, sensor (#2) shows significant and quick responses by the motion of the

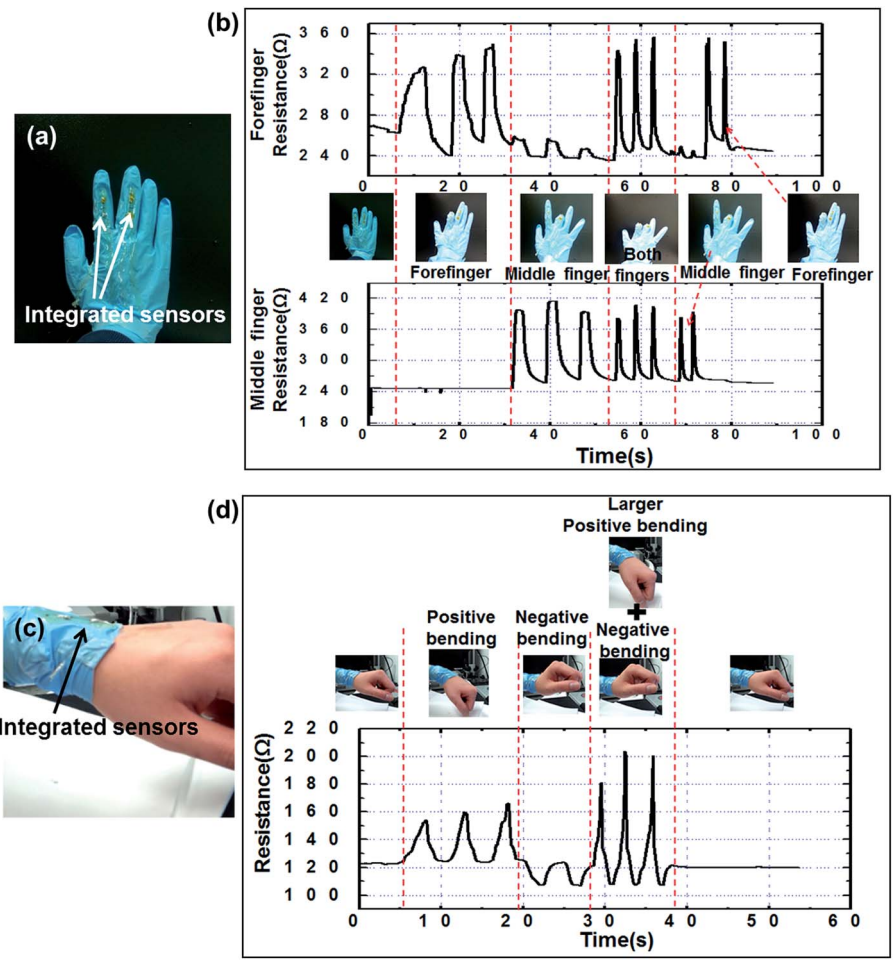

Fig. 5 Photograph image of (a) a motion detection glove and (c) a wrist guard with integrated strain sensors; sensing performance of the strain sensor on (b) the motion detection glove and (d) the wrist guard; strain sensors on the glove and wrist guard showed highly sensitive and quick responses to the motions of both the forefinger and the middle finger by positive bending, as well as both positive and negative bending motions of the wrist.

middle finger. Small signals from sensor (#1) during this period are due to the small motion of the forefinger caused by the middle finger motion. When both the forefinger and middle finger moved at the same time, both sensors rapidly responded to their repeated bending/relaxation motions. This result indicates the excellent performance of developed Ag NP based strain sensors for the flexible and wearable glove system for human finger motion detection.

The motion of the wrist involves both positive and negative bending at the joint, which means that both tensile and compressive strains can be induced on the surface. Since our sensor can detect both tensile and compressive strains, they were used for the detection of the wrist motion. As shown in Fig. 5c and d, the strain sensor was integrated onto the top surface of the wrist band and the sensing performance was measured. When the wrist was bent downward (positive bending) with induced tensile strain to the sensor, the resistance of the sensor was increased. Then, the resistance of the sensor was recovered by moving the wrist back to the initial state. Also, the sensor showed repeatable sensing performance under repeated bending/relaxation cycles. On the other hand, when the wrist was bent upward, the resistance of the sensor was decreased due to the induced compressive strain by the negative bending of the sensor. The sensor response to repeated cycles of larger positive bending and negative bending motions of the wrist was also measured. The resistance of the sensor was sharply increased during the positive bending periods and then was decreased lower than the initial resistance value during the negative bending periods. From these motion detection results, we demonstrated that our sensor can be applicable to the real-time and parallel sensing of multiple human motions with a large range of strains. Also, we used the strain sensor for detecting the motion of Adam's apple caused by spittle swallowing. The repeated tiny motions of Adam's apple by swallowing spittle resulted in the contraction of the skin and thus induced the decrease of the electrical resistance of the strain sensor (see ESI, Fig. S5†).

Furthermore, as another application, we used our sensor as the flexible pressure sensor. Flexible pressure sensors have several advantages such as mechanical flexibility, shock resistance and compatibility with non-flat surfaces. Therefore, various flexible pressure sensors have been studied for applications in medical and industrial fields.[30–34] In this work, we utilized a thin PDMS membrane (thickness = 100–500 μm) as a deformable diaphragm and an Ag NP based serpentine metallic pattern as the piezoresistive element to implement a flexible pressure sensor device. The working principle of the fabricated flexible pressure sensor is shown in Fig. 6b. An upward deflection of the membrane by positive pressure causes tensile strain of the PDMS membrane, resulting in the increase of the resistance of the Ag NP thin film. Fig. 6c shows the sensing performance of the flexible pressure sensor with a 100 μm thick PDMS membrane for 1 kPa input pressure. The pressure sensor showed a fast response (~1 s) and recovery (~0.5 s) speeds with high sensitivity ($\Delta R/R_0 = 0.35$) and the sensing performance was uniform under repeated on/off cycles of the input pressure. As shown in Fig. 6d, the response ($\Delta R/R_0$) to a pressure of 3 kPa for

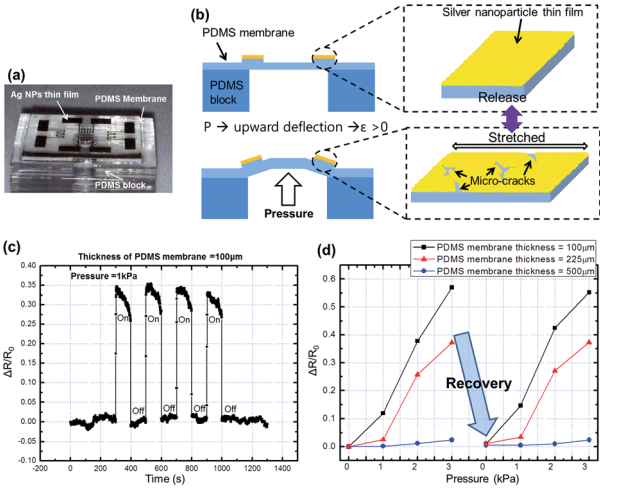

Fig. 6 Flexible pressure sensor: (a) the photograph of the fabricated flexible pressure sensor on the PDMS block, (b) the working principle of the flexible pressure sensor, (c) sensing performances of the pressure sensor with a 100 μm thick PDMS membrane under a pressure of 1 kPa, and (d) sensing performances of the pressure sensor with various PDMS membrane thicknesses (100, 225, 500 μm) under a repeated pressure ranging from 1 to 3 kPa.

the sensor with a 100 μm-thick PDMS membrane was ~28 times higher than that of the sensor with a 500 μm-thick PDMS membrane due to much higher mechanical flexibility. Therefore, the sensitivity and operation range can be easily adjusted by controlling the thickness of PDMS membrane. We believe that our flexible pressure sensor can be used for detecting low pressure on the curved/non-flat surface in various applications such as blood pressure measurement on a stent and catheter, gas leakage detection on a curved pipe surface, *etc.*

4. Conclusions

In conclusion, we demonstrated a new type of highly flexible and stretchable strain sensor based on the Ag NP thin film on the PDMS substrate using the single-step direct transfer process of ion-based Ag nano-ink. This fabrication method is very simple with a fast fabrication speed and a low manufacturing cost. The opening and closure of micro-cracks on the Ag NP thin film by elongation/relaxation cycles enable high stretchability and sensitivity of the sensor. The strain sensor showed excellent sensing performance with fast response/recovery and high sensitivity under both tensile and compressive strains. Furthermore, the sensor exhibited good durability against repeated loading cycles and long-term stability against constant strain. We demonstrated that the developed strain sensor is applicable for detecting multiple human motions such as finger and wrist motions and for measuring the pressure with high sensitivity to a low pressure. It is believed that this Ag NP-based stretchable strain sensor can provide a very efficient and highly economic approach to enable the human motion, force and pressure measurement devices for the next-generation flexible and wearable electronic systems.

Acknowledgements

This research was supported by the Fundamental Research Program (PNK3771) of the Korean Institute of Materials Science (KIMS), Research Program (KM3330) of Korea Institute of Machinery & Materials (KIMM), and the Nano Material Technology Development Program through the National Research Foundation of Korea (NRF) funded by the Ministry of Science, ICT & Future Planning (no. 2013043661).

Notes and references

1 M. Koo, K. I. Park, S. H. Lee, M. Suh, D. Y. Jeon, J. W. Choi, K. Kang and K. J. Lee, *Nano Lett.*, 2012, **12**, 4810.
2 A. M. Gaikwad, G. L. Whiting, D. A. Steingart and A. C. Arias, *Adv. Mater.*, 2011, **23**, 3251.
3 M. Park, J. Im, M. Shin, Y. Min, J. Park, H. Cho, S. Park, M. B. Shim, S. Jeon, D. Y. Chung, J. Bae, J. Park, U. Jeong and K. Kim, *Nat. Nanotechnol.*, 2012, **7**, 803.
4 F. Xu, X. Wang, Y. Zhu and Y. Zhu, *Adv. Funct. Mater.*, 2012, **22**, 1279.
5 D. S. Gray, J. Tien and C. S. Chen, *Adv. Mater.*, 2004, **16**, 393.
6 V. F. Curto, C. Fay, S. Coyle, R. Byrne, C. O'Toole, C. Barry, S. Hughes, N. Moyna, D. Diamond and F. Benito-Lopez, *Sens. Actuators, B*, 2012, **171–172**, 1327.
7 H. Kudo, T. Sawada, E. Kazawa, H. Yoshida, Y. Iwasaki and K. Mitsubayashi, *Biosens. Bioelectron.*, 2006, **22**, 558.
8 S. Takamatsu, T. Kobayashi, N. Shibayama, K. Miyake and T. Itoh, *Sens. Actuators, A*, 2012, **184**, 57.
9 Y. Miyoshi, K. Miyajima, H. Saito, H. Kudo, T. Takeuchi, I. Karube and K. Mitsubayashi, *Sens. Actuators, B*, 2009, **142**, 28.
10 P. Tormene, M. Bartolo, A. M. D. Nunzio, F. Fecchio, S. Quaglini, C. Tassorelli and G. Sandrini, *BioMedical Engineering Online*, 2012, **11**, 95.
11 T. Giorgino, F. Lorussi, D. D. Rossi and S. Quaglini, *28th IEEE EMBS Annual International Conference*, New York City, 2006.
12 R. J. N. Helmer, D. Farrow, K. Ball, E. Phillips, A. Farouil and I. Blanchonette, *Procedia Eng.*, 2011, **13**, 513.
13 R. J. N. Helmer, D. Farrow, S. R. Lucas, G. J. Higgerson and I. Blanchonette, *Procedia Eng.*, 2010, **2**, 2985.
14 C. X. Liu and J. W. Choi, *J. Micromech. Microeng.*, 2009, **19**, 085019.
15 H. Maune and M. Bockrath, *Appl. Phys. Lett.*, 2006, **89**, 173131.
16 T. Yamada, Y. Hayamizu, Y. Yamamoto, Y. Yomogida, A. Izadi-Najafabadi, D. N. Futaba and K. Hata, *Nat. Nanotechnol.*, 2011, **6**, 296.
17 D. J. Lipomi, M. Vosgueritchian, B. C. Tee, S. L. Hellstrom, J. A. Lee, C. H. Fox and Z. Bao, *Nat. Nanotechnol.*, 2011, **6**, 788.
18 S. P. Lacour, D. Chan, S. Wagner, T. Li and Z. Suo, *Appl. Phys. Lett.*, 2006, **88**, 204103.
19 C. Mattmann, F. Clemens and G. Tröster, *Sensors*, 2008, **8**, 3719.
20 Y. J. Kim, J. Y. Cha, H. Ham, H. Huh, D. S. So and I. Kang, *Curr. Appl. Phys.*, 2011, **11**, S350.
21 M. Ying, A. P. Bonifas, N. Lu, Y. Su, R. Li, H. Cheng, A. Ameen, Y. Huang and J. A. Rogers, *Nanotechnology*, 2012, **23**, 344004.
22 X. Xiao, L. Yuan, J. Zhong, T. Ding, Y. Liu, Z. Cai, Y. Rong, H. Han, J. Zhou and Z. L. Wang, *Adv. Mater.*, 2011, **23**, 5440.
23 S. Kim, W. S. Lee, J. Lee and I. Park, *Nanotechnology*, 2012, **23**, 285301.
24 I. M. Graz, D. P. J. Cotton and S. P. Lacour, *Appl. Phys. Lett.*, 2009, **94**, 071902.
25 O. Graudejus, Z. Jia, T. Li and S. Wagner, *Scr. Mater.*, 2012, **66**, 919.
26 A. D. Drozdov, S. Clyens and N. Theilgaard, *Meccanica*, 2013, **48**, 2061.
27 A. Dorfmann and R. W. Ogden, *Int. J. Solids Struct.*, 2004, **41**, 1855.
28 S. Kim, S. Won, G. D. Sim, I. Park and S. B. Lee, *Nanotechnology*, 2013, **24**, 085701.
29 D. A. Gerard and D. A. Koss, *Mater. Sci. Eng., A*, 1990, **129**, 77.
30 C. Li, P.-M. Wu, L. A. Shutter and R. K. Narayan, *Appl. Phys. Lett.*, 2010, **96**, 053502.
31 A. T. Sepúlveda, A. J. Pontes, J. C. Viana, G. Villoria, F. Fachin, B. L. Warlde and L. A. Rocha, *33rd IEEE EMBS Annual International Conference*, Boston, 2011.
32 F. M. Yaul, V. Bulović and J. H. Lang, *J. Microelectromech. Syst.*, 2012, **21**, 897.
33 A. T. Sepúlveda, F. Fachin, R. G. d. Villoria, B. L. Wardle, J. C. Viana, A. J. Pontes and L. A. Rocha, *Procedia Eng.*, 2011, **25**, 140.
34 D. Ha, W. N. de Vries, S. W. John, P. P. Irazoqui and W. J. Chappell, *Biomed. Microdevices*, 2012, **14**, 207.